

# A Novel Tensile Strained Ge/InGaAs Quantum Well Laser for MIR Applications

Rutwik Joshi<sup>1</sup>, S. Johnston<sup>2</sup>, S. Karthikeyan<sup>1</sup>, and M. K. Hudait<sup>1\*</sup>

<sup>1</sup> Virginia Polytechnic Institute and State University, Blacksburg, VA 24061, USA

<sup>2</sup> National Renewable Energy Laboratory, Golden, Colorado 80401, USA

\*E-mail: mantu@vt.edu

## Abstract

A tensile strained Ge/InGaAs quantum well (QW) laser is proposed and evaluated using in-house materials growth and characterization results feeding to TCAD solvers. This  $\epsilon$ -Ge/InGaAs laser provides type-I band alignment with high valence band and conduction band offsets, along with high minority carrier lifetime. At indium (In) = 28% in InGaAs, the  $\epsilon$ -Ge active layer is a direct-gap material due to the tensile strain and lasing is possible at a wavelength of  $\sim 2.1 \mu\text{m}$  with a threshold current density  $\sim 6 \text{ kA/cm}^2$ , an improvement over existing Ge lasers and comparable to direct gap MIR lasers. The high band offsets and carrier lifetime enable this  $\epsilon$ -Ge QW laser to provide a high net material gain of  $1211 \text{ cm}^{-1}$  with an improved efficiency of 20 %.

## 1. Introduction

Germanium-based nanoscale transistors have the potential to boost the performance of conventional Si-based devices which are nearing a performance roadblock [1]. Beyond electronics, the need for communication and computational performance can be satisfied by photonics and quantum technologies. An electrically powered laser is a key component for on-chip sensing, quantum computation, and photonics. The tensile strained germanium ( $\epsilon$ -Ge) is a suitable solution due to: (i) the direct bandgap of Ge is in the  $\sim 1550 \text{ nm}$  range compatible with optical communication platforms [2], (ii) the band gap of Ge is tunable with strain [1,3], (iii) compatibility with modern Si-based infrastructure, and (iv) ability to form high-performance control circuits and logic [1]. Furthermore, because of the capacity crunch in the OFC spectrum, utilizing the  $2 \mu\text{m} - 4 \mu\text{m}$  range may be needed [4,5]. Additionally, the mid-infrared (MIR) regime could be useful to integrated Si-optics, quantum metrology, and sensing due to the reduced linear and nonlinear losses. Here, we present a novel strained Ge-based quantum well (QW) light source that can be grown monolithically on GaAs or Si substrate through a lattice-

graded buffer. The defects in the active layer are reduced substantially and the quality of the  $\epsilon$ -Ge QW lasing medium is evaluated through the minority carrier lifetime, to be as high as 64 ns. The band alignment measured using x-ray photoelectron spectroscopy (XPS) as a function of indium (In) composition [6-9] in InGaAs, along with the carrier lifetime are fed to the calibrated TCAD solver to calculate the lasing spectra and electrical performance. The electrical quantum-corrected TCAD solver have previously been calibrated for nanoscale devices [1].

## 2. Structure, Growth, and Characterization

The structure of the proposed  $\epsilon$ -Ge/InGaAs QW laser is shown in Fig. 1. The growth of high quality  $\epsilon$ -Ge/In<sub>x</sub>Ga<sub>1-x</sub>As QW structure is achieved via vacuum interconnected solid source MBE [3], [6-9] on a GaAs or Si substrate using a lattice grading buffer to mitigate defects. This pseudomorphic growth of virtually defect-free  $\epsilon$ -Ge on In<sub>x</sub>Ga<sub>1-x</sub>As is possible provided the  $\epsilon$ -Ge is thinner than the critical thickness [10]. The AlGaInAs quaternary layer forms the separate confinement heterostructure (SCH) Q-barrier [3]. The band alignment is a critical attribute of a QW laser, the valence band offset ( $\Delta E_V$ ) for various In compositions [6-8] is measured through XPS, and the corresponding conduction band offsets ( $\Delta E_C$ ) are calculated using a 6x6 k.p band calculation tuned to match 30x30 k.p [3]. The band offsets are high and a type I alignment is obtained, indicating good carrier confinement

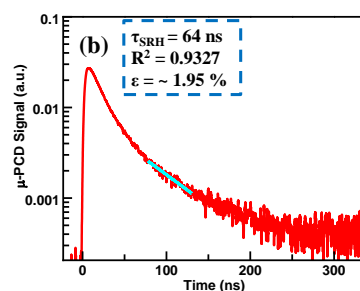


Fig. 2. Measurement of minority carrier lifetime using PCD for 1.95 % tensile strained Ge/InGaAs QW, indicating an improved IQE.

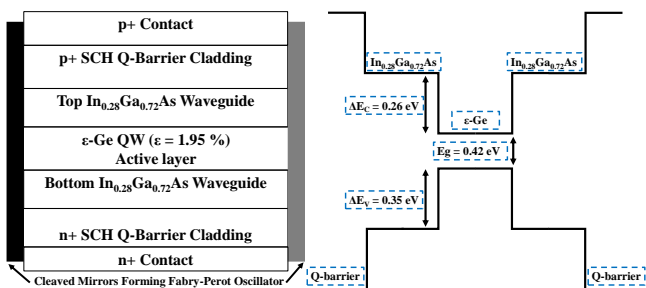


Fig. 1. Schematic of the proposed 1.95 % tensile strained Ge/InGaAs SCH QW (left) and band alignment (right).

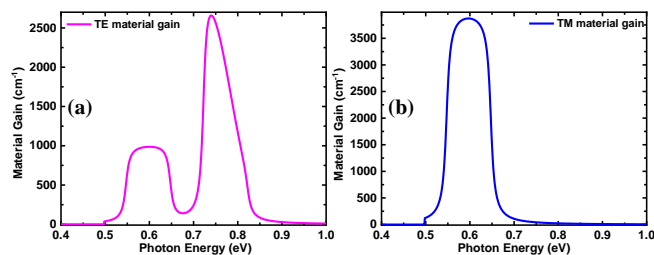
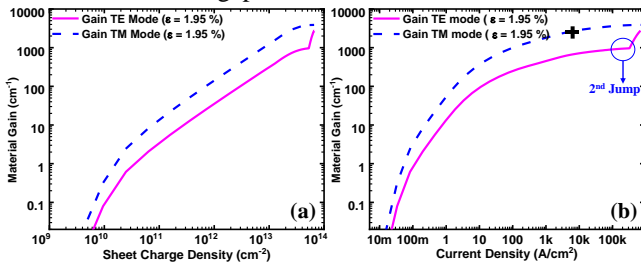


Fig. 3. Gain spectrum at In = 28 % corresponding to a tensile strain of 1.95 % in Ge QW for the (a) TE and (b) TM modes.

at 300K. The band offsets are used for calibration of the simulation framework to accurately predict the QW attributes. The material quality for the 1.95%  $\epsilon$ -Ge QW is assessed through the microwave photoconductive decay ( $\mu$ -PCD) method [11]) with a 1500 nm laser and an injected carrier density of  $\sim 10^{13} \text{ cm}^{-3}$  with the excitation power  $\sim 2 \text{ mW}$ . PCD lifetime value (64 ns, *see* Fig. 2) for the Shockley–Read–Hall (SRH) recombination is fed to the TCAD [12] solver. Also, other non-radiative recombination mechanisms such as Auger processes are included in the calibrated model. Due to the high minority carrier lifetime, the SRH recombination is non-dominant, but the Auger recombination would be significant due to the low band gap of  $\epsilon$ -Ge.



**Fig. 4.** Material gain as a function of injected (a) carrier and (b) current density for the TE and TM modes for direct gap  $\epsilon$ -Ge at In = 28 %.

### 3. Lasing Performance of the Ge QW

The lasing spectra for the transverse electric and magnetic (TE and TM) modes are calculated in a two-step process: (i) the measured carrier lifetime, structure, composition, strain, and band alignment are fed to TCAD solver and (ii) the electrical metrics are fed to an in-house laser-gain solver for computation of lasing performance [13,14]. Note that higher-order modes will exist in the cavity, and the optical emission will be either quasi-TE or quasi-TM, but the analysis here is performed only for the fundamental modes. The SCH QW cavity is designed to maximize the optical confinement. The Ge QW emission spectrum for the material gain is shown for the TE and TM modes for a tensile strain of 1.95 % in Fig. 3 for a QW thickness of 7 nm. Due to the LH-HH band split associated with the biaxial tensile strain in Ge, the dominant emission is TM mode. A high TM material gain of  $3873 \text{ cm}^{-1}$  is obtained for the TM mode for an emission wavelength of  $\sim 2.1 \mu\text{m}$ . The TE and TM material gain as a function of injected carrier density and current density are shown in Fig. 4(a) and (b), respectively. It can be noticed that the TM mode provides higher material gain at much lower injected current densities compared to the TE mode. Considering a free carrier absorption of  $500 \text{ cm}^{-1}$  and a mirror loss of  $25 \text{ cm}^{-1}$ , a net TM material gain of  $1211 \text{ cm}^{-1}$  corresponding to a net TM modal gain of  $14 \text{ cm}^{-1}$  is attained at a lasing threshold of  $6 \text{ kA/cm}^2$  (*see* Fig. 4b with “+” sign indicating  $J_{\text{TH}}$ ). Whereas the TE mode is not able to cross the lasing threshold by overcoming the losses in the cavity. Due to the significant population in the indirect L-valley even when Ge is a direct gap active layer at  $\epsilon = 1.95 \%$ , the  $J_{\text{TH}}$  has a lower limit. The radiative transitions are made more probable due to the tensile strain and corresponding lowering of the  $\Gamma$ -valley. Furthermore, due to the high carrier lifetime, the SRH non-radiative recombination is minimized. Thus, the internal quantum efficiency is

boosted to  $\sim 20 \%$  for this  $\epsilon$ -Ge QW configuration despite the dominant Auger recombination. The transition strength of the emission from the LH and HH bands will vary for the TE and TM modes as a function of the band structure. As the TM mode gain originates primarily from the LH band, the gain peak remains around  $0.58 \text{ eV}$  corresponding to the  $\Gamma$ -LH separation for all applied bias (*see*, Fig 5(a)). But, for the TE mode gain, at very high injection, the fermi level separation is sufficient to excite the carrier in the HH-band as well. Due to the high DOS associated with the HH-band, the TE gain is dominated by the  $\Gamma$ -HH emission at high injection resulting in two distinct energy peaks and a bias-dependent emission spectrum as shown in Fig. 5(b).

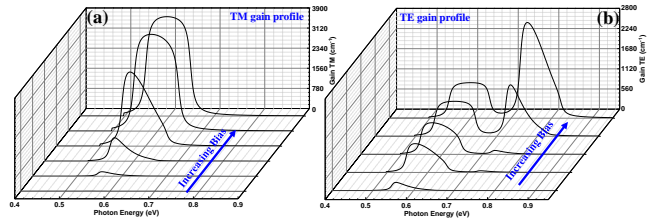


**Fig. 5.** Bias dependence at In = 28 % for the (a) TM and (b) TE mode gain for the  $\epsilon$ -Ge QW laser.

### 3. Conclusions

Through calibrated TCAD solver and in-house experiments; the lasing spectra, polarization, and electrical performance of the proposed  $\epsilon$ -Ge/InGaAs QW laser are analyzed. It is observed that the  $\epsilon$ -Ge/InGaAs QW laser can provide efficient lasing attributed to the direct band gap  $\epsilon$ -Ge active layer, high carrier lifetime, and band offsets. A high net TM material gain of  $1211 \text{ cm}^{-1}$  is achieved for a single QW configuration at an operating wavelength of  $2.1 \mu\text{m}$  with a lasing threshold of  $6 \text{ kA/cm}^2$ . Thus, explorations in tensile strained Ge/InGaAs SQW and MQW SCH cavities are an interesting avenue for application in on-chip MIR photonics and quantum technologies.

### Acknowledgements

Authors acknowledge support from the NSF under grant number ECCS- 2042079, a US-Ireland joint R&D program.

### References

- [1] R. Joshi, S. Karthikeyan, and M. K. Hudait, *IEEE Trans. Electron Dev.*, **69**, 4175-4182, 2022.
- [2] K. Tani, T. Okumura, K. Oda, M. Deura, and T. Ido, *Opt. Express* **29**, 28021-28036, 2021.
- [3] M K Hudait, *et al.*, *ACS Appl. Electron. Mater.*, **3**, 4535–4547, 2021.
- [4] D. J. Richardson, *Science* **330**, 327–328, 2010.
- [5] E. Agrell, *et al.*, *J. Opt.*, **18**, 063002, 2016.
- [6] M. K. Hudait, Y. Zhu, N. Jain, and J. L. Hunter, Jr, *J. Vac. Sci. Technol. B* **31**, 011206, 2013.
- [7] M. Clavel, *et al.*, *ACS Appl. Mater. Interf.*, **7**, 26470–26481, 2015.
- [8] Y. Zhu, *et al.*, *ACS Appl. Mater. Interf.*, **6**, 4947 - 4953, 2014.
- [9] M. Clavel, P. Goley, N. Jain, Y. Zhu, and M. K. Hudait, *IEEE J. Electron Dev. Soc.*, **3**, 184-193, 2015.
- [10] M. B. Clavel, *et al.*, *Phys. Rev. Appl.*, **18**, 064083, 2022.
- [11] S. Johnston, *et al.*, *IEEE J. Photovolt.*, **4**, 1295-1300, 2014.
- [12] TCAD Sentaurus Device Manual Release: T-2022.03, Synopsys Inc.
- [13] L. A. Coldren, S. W. Corzine, M. L. Mašanović, Diode Lasers and Photonic Integrated Circuits, John Wiley & Sons, 2012.
- [14] Y. Arakawa and A. Yariv, *IEEE J. Quantum Electron.*, **21**, 1666-1674, 1985.